Indian Journal of Engineering & Materials Sciences
Vol. 27, December 2020, pp. 1071-1079

Stable ensemble brightness from nitrogen vacancy centers in nanodiamonds through optimized surface composition

Sandeep[b], Ravi Kumar[a,b], Kiran Mahadeo Subhedar[a,b], Raj Kumar[c] & Sanjay Rangnath Dhakate[a,b*]

[a]Academy of Scientific and Innovative Research (AcSIR), Ghaziabad, Uttar Pradesh 201 002, India

[b]CSIR-National Physical Laboratory, Dr K S Krishnan Marg, New Delhi 110 012, India

[c]Inter University Accelerator Centre, Aruna Asaf Ali Marg, New Delhi 110 067, India

Received:25 August 2020

Stable ensemble emission from nitrogen vacancy (NV) centers in nanodiamonds (NDs) is highly desirable for diverse areas ranging from bio-imaging to quantum optics. The uniqueness of NV centers lies in their opto-spin properties like energy level structure, emission range (620-850 nm) and optical spin polarization. The host matrix (NDs), however, put some limitation on the photo-physical properties of these color centers. One of the major issues is surface proximity (where high concentration of defects are present) of NV centers. The NV centers being highly sensitive to the neighboring environment are unstable in such circumstances. The surface of NDs mainly exhibit non-diamond carbon which is well-known quencher of emission due to NV centers. The surface composition for desirable photo-physical properties of NV centers is still unknown. Here, we have systemically studied the effect of oxidation time at low oxidation temperature (450 ^{o}C) on the selective removal of sp^2 carbon, aqueous dispersion of NDs and emission collection due to NV centers at ensemble level. Among different air oxidations, heat treatment at 450 ^{o}C at residual time of 8 hours has been found to be suitable air oxidation conditions for the enhancement of brightness and ensemble photo-stability of NV centers.

Keywords: Nanodiamonds, Nitrogen vacancy centers, Air oxidation, Ensemble photo-stability

1 Introduction

Diamond is very wide band gap semiconductor (E_g~5.5 eV) with a large number of point defects (> 500) having distinct optical and spin properties[1-3]. Among these point defects (color centers), the nitrogen vacancy centers (NV) contain exceptional combination of optical and spin properties[4,5]. The NV centers have been identified mainly in two different charge states: neutral (NV^o) and negative (NV^-). The NV^o center has zero photon line (ZPL) around 575 nm and NV^- center has ZPL around 637 nm. The combined side band emission of NV centers lies from 550-850 nm[4]. Among different charge states, the NV^- centers are at the center of all research attention due to its energy level structure (ground and excited state spin triplet and intermediate singlet state)[5,6]. Due to optical spin polarization of ground state (m_s=0), the NV^- centers exhibit optically detected magnetic resonance (ODMR)[5,7]. The ODMR leads to a large number of quantum sensing protocols ranges from condensed matter physics to biological sciences[1, 8-11]. The NV^- centers behaves like single atomic system in inert diamond matrix whose phonons do not interact with the electrons of the defects (low electron-phonon interaction). All the properties of NV^- centers are unchanged when the host matrix reduced to nanoscale[12]. The NDs inherits all the properties of diamond with the advantage of easy surface tailoring as well as penetration in different nanoscale physical systems as in-situ probe[13].

One limitation of the NV^--NDs system is the presence of non-diamond carbon at the surface[14]. These carbon phases are not converted in to diamond during growth and appear at the surface of ND particles[15]. Due to the fact that the size of NDs is usually ≤ 100 nm, there is always proximity of surface and NV^- centers. The surface non-diamond carbon and defects are source of spin noises, electron traps and absorption of NV emission[16,17]. This leads to fast quenching as well blinking of NV centers in addition to weak emission collection. Hence, the surface engineering is of utmost importance before the application of NDs. There are different techniques for the selective removal of non-diamond carbon and functionalization of the surface of NDs[13,18]. Among different conventional purification techniques for

*Corresponding author (E-mail: dhakate@nplindia.org)

selective removal of non-diamond carbon and defects, the air oxidation has been found to be more efficient[18]. On the other hand, the acid refluxing leads to higher surface functionality as well as aqueous dispersion of NDs[17-19]. Accordingly, the removal of non-diamond carbon is generally carried out through one step air oxidation at elevated temperature (≥ 500° C)[20, 21]. This simultaneously leads to nearly complete removal of non-diamond carbon as well as appearance of oxygen functionality at the surface[19]. However, it has been reported that very high degree of oxidation is also detrimental to the ensemble photo-stability of NV centers[19]. Also, the output yield of this purification method is very low. Hence, the optimized surface for bright and stable emission due to NV centers is still undetermined.

Here, we have explored the effect of oxidation time (2-8 hours) at constant temperature of oxidation (450° C) on the brightness and ensemble photo-stability of NV centers. The emission collection, ensemble brightness and photo-stability of NV centers have been analyzed through PL spectroscopy and confocal microscopy. It turned out that air oxidation at 450° C for 8 hours is suitable oxidation temperature to increase the emission collection due to NV centers as compared to heat treatment at still higher temperature where emission blinking is generally observed.

2 Experimental Details

2.1 Air oxidation of nanodiamonds

The initial material (element six, MICRON + MDA M0.10) was purchased from element six. It was termed as S1. The sample S1 was heat treated at 450° C at different residual time in quartz reactor under the ambient air flow in tubular furnace. The residual time of heat treatment at 450° C was 2-8 hours (Fig. 1). The Raman and PL spectra were recorded for each different oxidized sample. The samples were termed as S2 (oxidation time 2 hours), S3 (oxidation time 4 hours), S4 (oxidation time 4 hours) and S5 (oxidation time 8 hours).

2.2 Characterizations

The Raman and PL spectroscopy were carried out with Renishaw in *via* spectrometer in back scattered geometry (50X objective). The laser excitation wavelength of 514 nm was used for the Raman and PL spectroscopy. The Raman and PL spectra were deconvoluted with Lorentzian line shape (Origin 9) and Guassian line shape respectively. The confocal microscopy was carried out with Olympus confocal system using 60X objective lens with oil immersion. The excitation wavelength of 488 nm was used for confocal imaging. The emission collection range was 550-650 nm. The confocal time lapse measurement was carried out under continuous laser excitation. The confocal images at different time were analyzed through Image J software to evaluate the change in brightness with time. In this way, the ensemble photo-stability of different samples was analyzed. The X-ray diffraction (XRD) was recorded with X'Pert Pro PAN analytical X-ray diffractometer and Cu-Kα (Wavelength=1.54059 Å). The XRD micrographs were deconvoluted with Voigt line shape. The atomic force microscopy (AFM) was carried out using NT -MDT SolverP47-Pro AFM system. The AFM analysis was carried out using WSxM software. The X-ray photoelectron spectroscopy (XPS) was carried out using XPS system Multi Lab 2000 spectrometer (Thermo Electron Corporation, England) equipped with Al kα as X-ray source. The XPS analysis of different

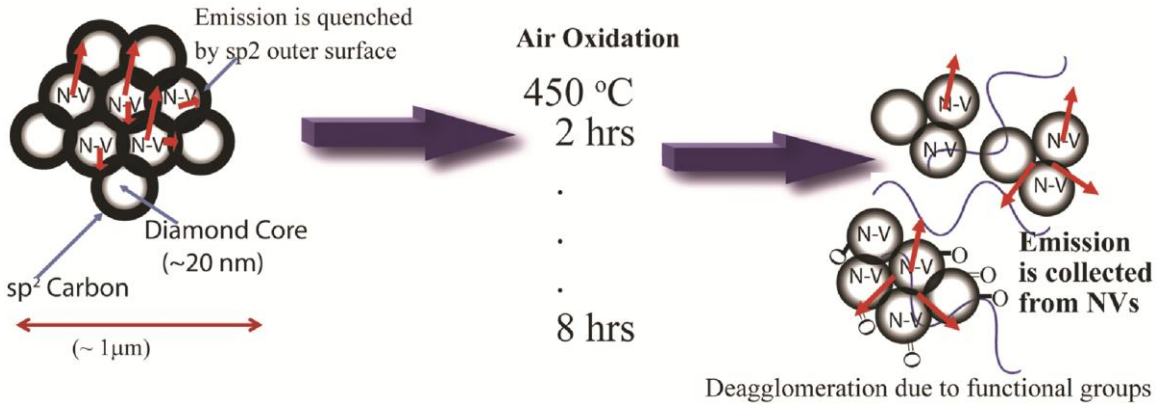

Fig. 1 — Schematic diagram showing the experimental details for the air oxidation of NDs under different conditions.

samples was carried out using XPS peak 4.1 software using Shirley background and Gaussian-Lorentzian line shape.

3 Results and Discussion

Figure 2 shows the AFM analysis of NDs before and after air oxidation. Figure 2(a) shows the AFM image of as purchased sample (S1). The NDs showed agglomeration and there was uneven dispersion over the substrate. It is due to the fact that the surface of NDs exhibits non-diamond carbon which leads to inter-particle bonding of varying strength. In addition, there was absence of functionality which caused the agglomeration and uneven morphology of NDs. The average particle size of sample S1 was calculated as 56.5 ± 24.8 nm. The standard deviation showed the large range of the particle size. The maximum and minimum particle sizes were found to be ~ 130 nm and ~ 17.9 nm respectively. Figure 2(b) shows the AFM image of sample oxidized for 8 hours (S5). As seen in the figure, the NDs were uniformly dispersed over the substrate. The average particle size of NDs were found to be 41.7 ± 13.3 nm. The standard deviation showed the narrow range of particle size. The maximum and minimum particle sizes were found to be ~ 78.1 nm and ~ 12.2 nm respectively. Figure 2(c) shows the possible mechanism for higher and uniform dispersion of particles. Due to the presence of different oxygen functionalities, there was electrostatic interaction of different NDs with water molecules which leads to higher and uniform degree of dispersion as compared to as received sample. Figure 3 shows the Raman spectra and X-ray diffraction (XRD) micrographs of different air oxidized NDs in comparison to as received NDs. Figure 3(a) shows the Raman spectra for different samples. In all the samples, the characteristic diamond peak was observed around 1332 cm^{-1} with varying intensity. There is also the presence of G and D-band due to sp^2 carbon and defects respectively. The intensity of G-band was decreasing with the increasing oxidation time. For sample oxidized for 8 hours, the G-band was vanished. Keeping in view that the Raman scattering cross-section of graphitic

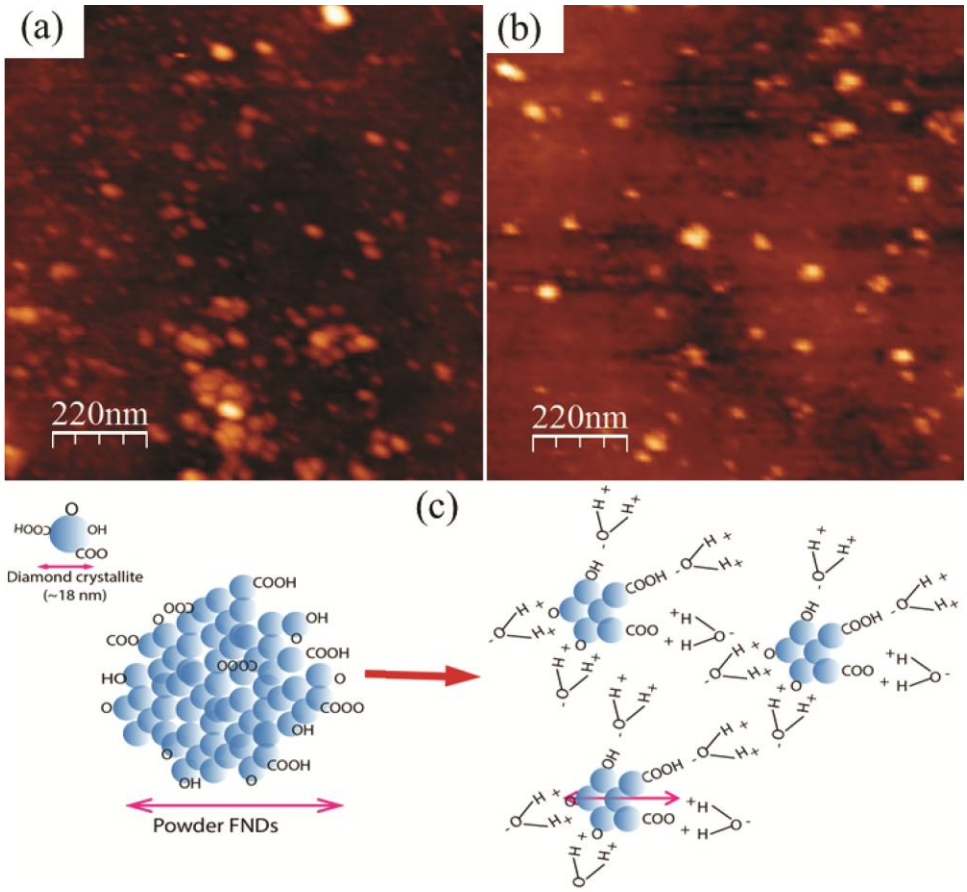

Fig. 2 — AFM analysis of air oxidized NDs (a) As received NDs, (b) air oxidized NDs for 8 hours (S5) and (c) The aqueous dispersion of air oxidized NDs is due to presence of oxygen functionalities at the surface.

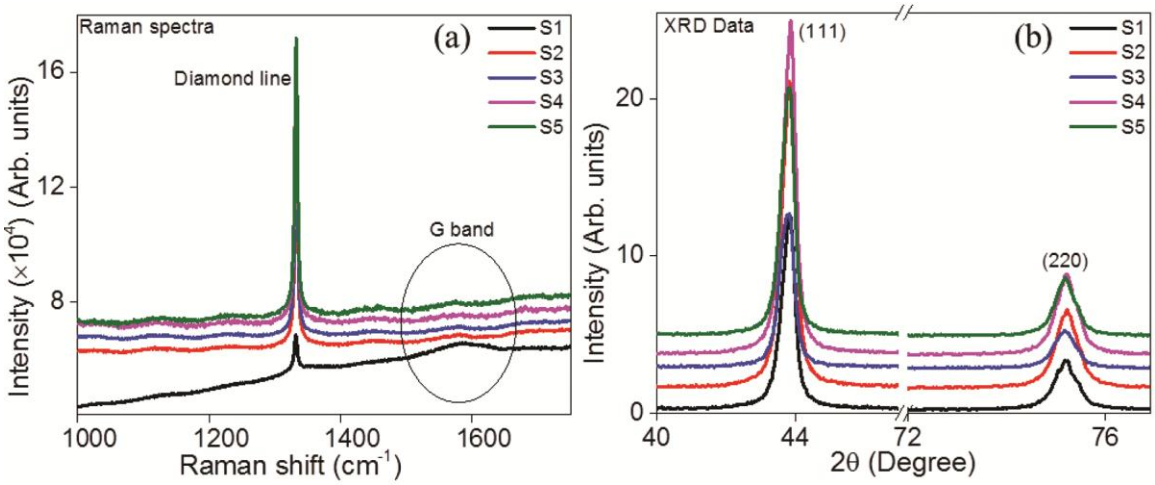

Fig. 3 — (a) Raman spectra for different air oxidized NDs. The black ellipsoid underlines the decreasing G band with the increasing oxidation time and (b) XRD micrographs for different NDs.

carbon is around 50 times higher as compared to diamond sp^3 carbon for excitation wavelength in visible range; the non-diamond carbon has been efficiently removed from the sample[22]. Also, Raman spectroscopy is bulk characterization technique having penetration depth of ~ 50 nm for graphite[23]. In our case, the graphitic carbon was localized to the surface of NDs. Hence, the penetration depth of Raman excitation laser in NDs was always more than 50 nm keeping in view that diamond is transparent to excitation laser whose wavelength lies in visible range. Hence, the air oxidation leads to drastic reduction of non-diamond carbon in NDs at bulk level. Figure 3(b) shows the XRD micrographs of different NDs. The characteristic (111) and (220) planes of diamond structure were observed in all the samples showing that the air oxidation does not affect the crystallinity. The (111) peak was used for the determination of average particle sizes (using Scherrer equation). The average particle size for as received NDs (S1) was ~19.5 nm and ~19.7 nm for oxidized sample (S5). Hence, the air oxidation does not etch the diamond lattice and its effects are localized to surface.

The surface compositions of different NDs were analyzed using XPS. Figure 4(a) shows the XPS survey scan of S1 and S5 samples. The carbon and oxygen were mainly present in both of the samples in addition to negligible presence of nitrogen (Fig. 4(a)). Figure 4(b) shows the *C1s* core spectra for different samples. The sample S1 exhibited higher *C1s* peak intensity as compared to S5. It is due to air oxidation which leads to the elimination of non-diamond carbon atoms and enhance the oxygen concentration near the surface. In case of sample S5, the carbon content near the surface was reduced and oxygen is increased in the penetration depth of X-ray as seen in *O1s* core spectra (Fig. 4(c)). For sample S1, the *C1s* and *O1s* peaks are observed around ~ 286 eV (FWHM ~ 2.5 eV) and ~ 533 eV (FWHM ~ 3.3.eV) respectively. In case of sample S5, *C1s* core and *O1s* core were present around ~ 287 eV (FWHM ~ 2.6 eV) and 533.6 eV (FWHM ~ 2.2 eV) respectively. The *C1s* core has been shifted toward higher binding energy side in case of oxidized sample probably due to insulating nature of this sample in comparison to S1 in which the surface was conducting due to presence of graphitic carbon. The charging effect would lead to shifting of binding energy toward higher side. Also, the FWHM of oxidized sample was higher as compared to initial sample. It was due to the fact that carbon-oxygen functionalization near the surface leads to the contribution of C=O bonds in the *C1s* core spectra toward higher binding energy side which ultimately caused the broadening of *C1s* core. Also, the presence of carbon-oxygen functionality leads to asymmetry in the *C1s* core in case of oxidized sample. Figure 4(d) shows the *N1s* core spectra for S1 and S5. In case of sample S1, a weak *N1s* peak was observed around ~ 400 eV, showing the presence of nitrogen atoms near the surface. The *N1s* peak has been completely disappeared in case of oxidized sample. The *N1s* peak S1 sample appeared probably due to chemical purification treatment by the manufacturer which caused the appearance of nitrogen functionalities on the surface of NDs.

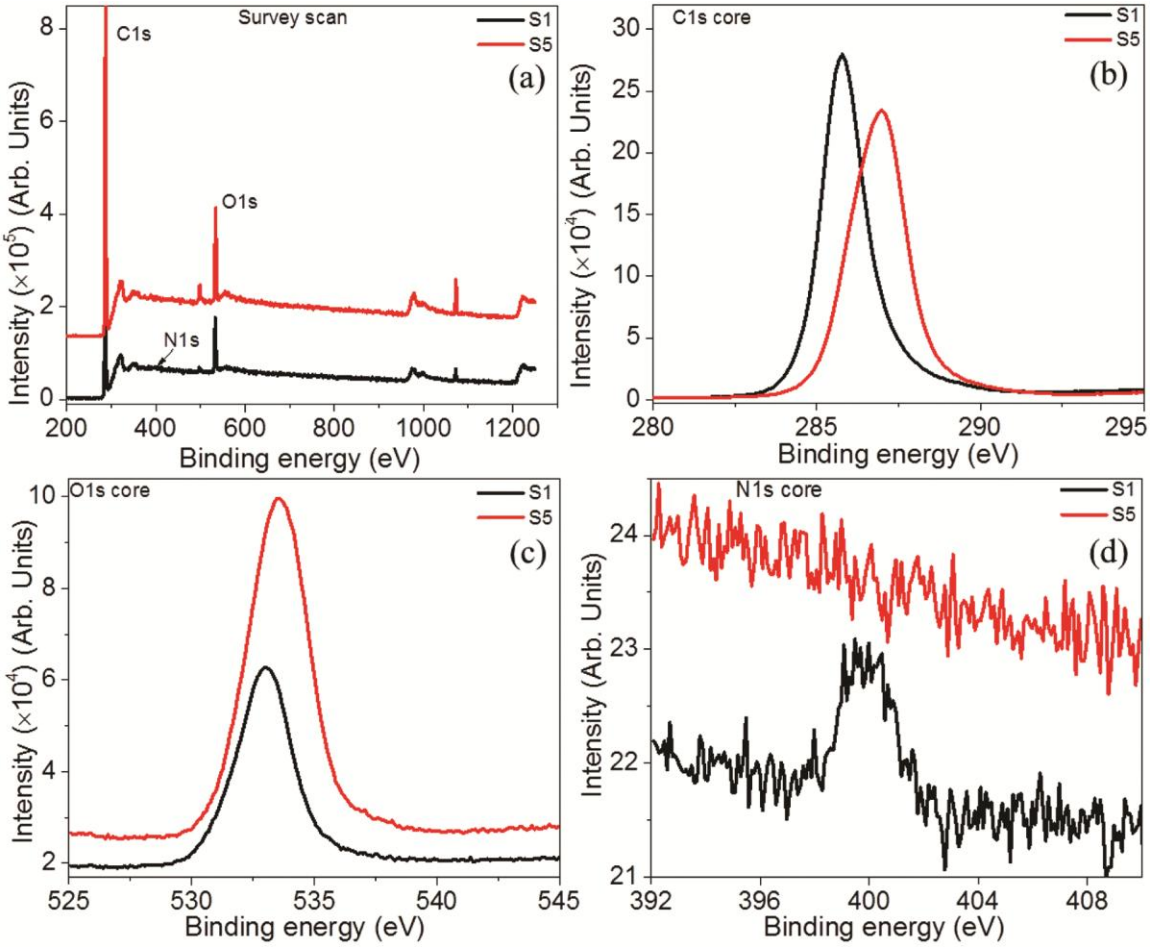

Fig. 4 — XPS analysis of S1 and S5 samples. (a) Survey scan; which show the presence of carbon and oxygen near the surface of NDs. (b), (c) and (d) show the *C1s*, *O1s* and *N1s* core spectra respectively for different samples.

Since, the air oxidation leads to reconstruction of the surface, these nitrogen functionalities detached from the surface and *N1s* peak disappeared. The XPS elemental composition analysis shows that the Sample S1 contains carbon, oxygen and nitrogen atoms in 88.15 atomic %, 9.4 atomic % and 1.49 atomic % respectively. In addition, sodium atoms were also present with around 0.96 atomic % in S1 sample. In case of sample S5, the carbon, oxygen and nitrogen atoms were present in 84.76 atomic %, 12.69 atomic % and 0.52 % respectively. In addition, sodium was also present in 2.03 atomic %. The nitrogen atoms were drastically reduced in the oxidized sample in comparison to initial sample and amount of sodium was increased.

Figure 5(a) shows the fitted *C1s* core spectra for initial as well as air oxidized sample. The initial sample exhibits p^2 carbon (~ 90%) and sp^3 carbon (~ 8 %) with negligible presence of oxygen functionalization. Hence, as far as XPS penetration depth is concerned, the initial sample exhibited highly graphitic environment. Whereas, the oxidized sample exhibit lower sp^2 (30.4 %) and higher sp^3 (60.1 %) carbon contents near the surface in addition to presence of carbon-oxygen functionality (C=O; 9.5 %).This clearly reflects the effect of selective air oxidation which have drastically reduced the near surface graphitic carbon from ~ 90 % to ~ 30.4 %. The reduction of non-diamond carbon was more efficient in the present case as compared to previous work where air oxidation was carried out without optimization under same oxidation temperature[18]. Figure 5(b) shows the *O1s* core spectra for different samples. As observed from the figure, both of the samples, S1 as well as S5, contain oxygen moieties like C-O, C=O and COO[24-26]. However, the concentration of different functionalities was changed due to air oxidation. In the initial sample, the

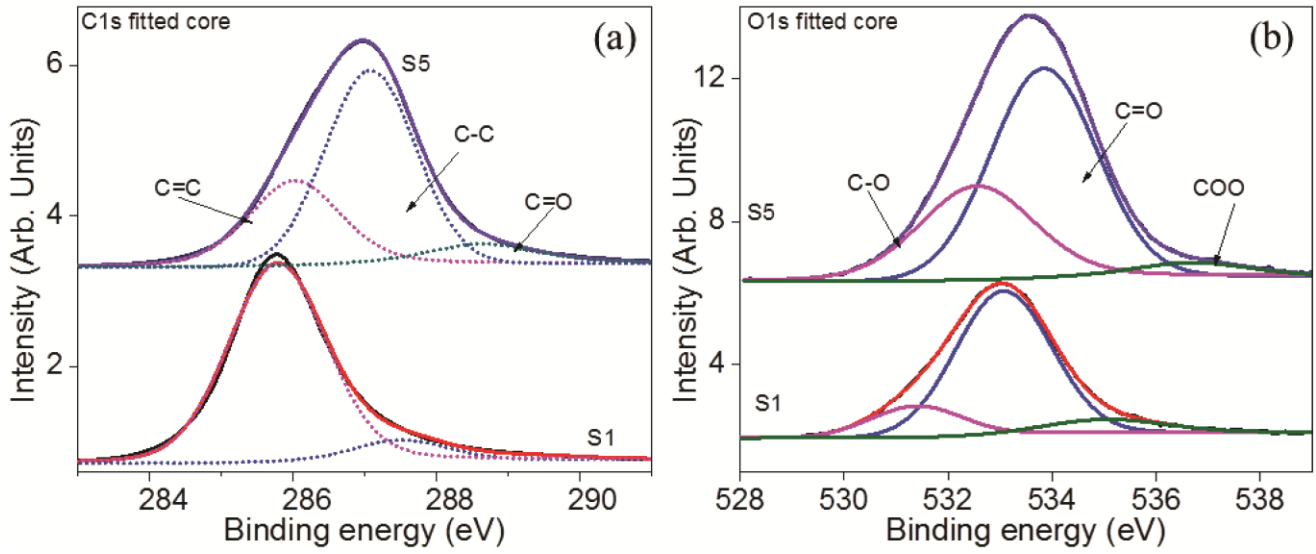

Fig. 5 — (a) Fitted *C1s* and (b) *O1s* cores for S1 and S5 samples.

carbonyl group (C=O; 75.8%) was mainly present in addition to small contribution due to alcoholic/ketone (C-O; 15.9%) and carboxylic/ester (COO; 8.3%). In case of oxidized sample, the C=O group was reduced to ~ 63.0 % and the concentration of C-O group has been increased to ~ 32.8 %. Also, the COO group was reduced to ~ 4.2 % in this sample as compared to S1. This was due to the fact that, C=O and COO groups involve sp^2 hybridized carbon atoms which are efficiently etched out during air oxidation. Simultaneously, the sp^3 carbon content is increased on the surface during air oxidation which in the presence of oxygen leads to the significant concentration of C-O group.

The PL measurements of all the samples were carried out under similar experimental conditions. To confirm that the exposure volume was same, different samples were prepared by spin coating the same amount of their aqueous solutions having exactly same concentration on acid treated silicon wafers. Also, the laser power and exposure time were same and all the samples were investigated in the single run of PL system. Moreover, the characteristic Raman line for Silicon wafer was also found to be absent in the PL spectra of all the samples indicating that the laser was completely absorbed by the sample and collection volume was nearly same. There is however, a small difference exist between the amount of sample volume exposed to the excitation laser due to varying concentration of sp^2 carbon in different samples (Fig. 3, Raman spectra). In commercially purchased sample, the sp^2 carbon content is very high which leads to absorption of laser by some finite volume of sample. In air oxidized samples, the sp^2 carbon concentration was decreased and sample's laser exposure volume is increased. In fact, the sample's laser exposure volume was inversely proportional to concentration of sp^2 carbon in the sample. The PL spectra of different air oxidized NDs are shown in Fig. 6(a). The as purchased sample exhibits no signs of characteristic NV emission and contained only broad and featureless emission in the wavelength range of 550-745 nm. On air oxidation for 2 hours, PL spectral shape was converted in to characteristic NV emission profile where the ZPL of NV^o and NV^- centers were observed around 575 nm and 637 nm, respectively, in addition to side bands. Most of the PL emission intensity was due to side band emission (very small Debye-Waller factor). The emission intensity is increasing with oxidation time (4 hours, 6 hours and 8 hours). However, there was only marginal increase in PL intensity after air oxidation at 6 hours. The maximum emission collection was achieved for sample oxidized for 8 hours (S5). Figure 6(b) shows the fitted PL spectra for sample S5. The ZPL emission of NV^o and NV^- centers was clearly observed in addition to prominent side bands. In order to compare the emission intensity in the ZPLs in different samples, the PL spectra in the wavelength range of 570-580 nm (NV^o centers) as well as 630-640 nm (NV^- centers) were compared for different samples (Fig. 6(c)). As seen in the figure, the ZPL intensity of both NV^o as well as NV^- centers increases with increasing heat treatment time. The ZPL intensity of

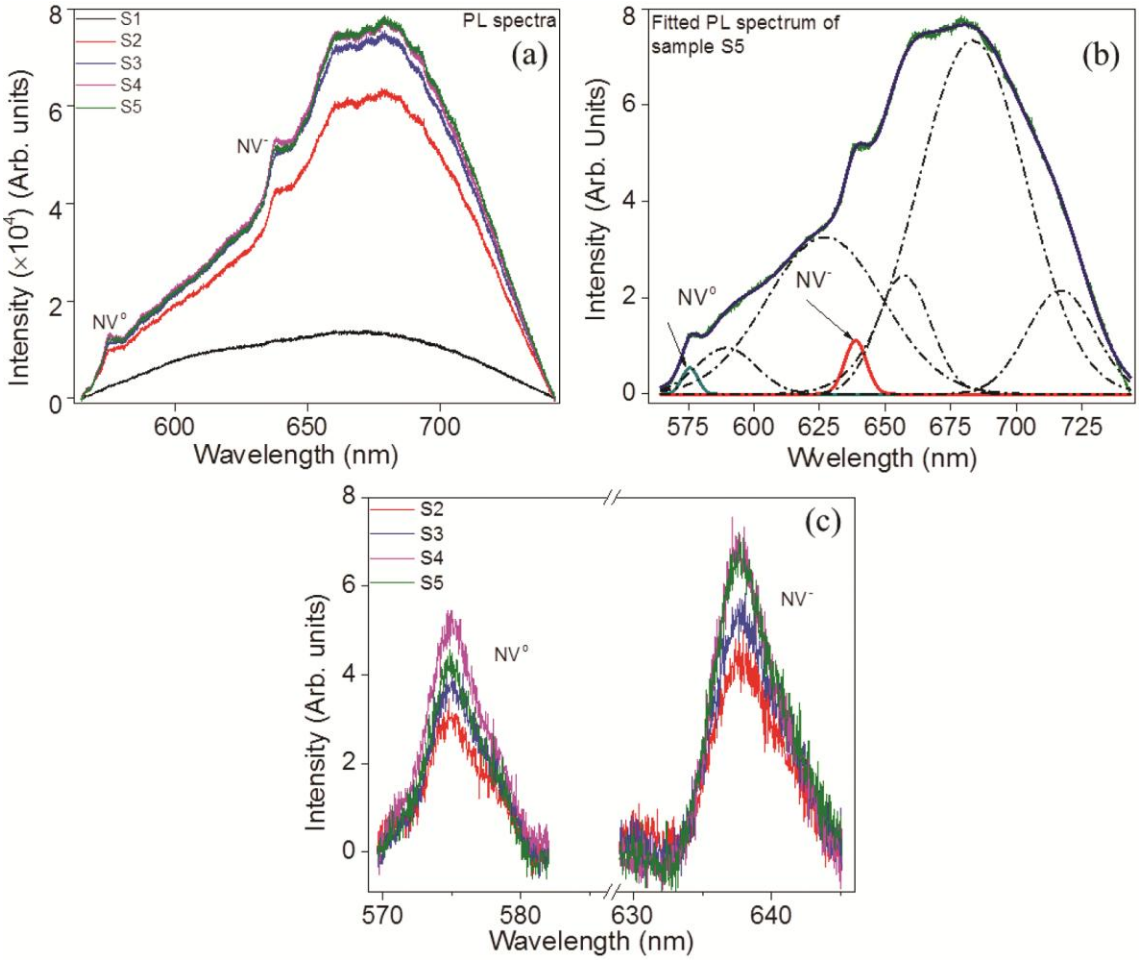

Fig. 6 — (a) PL spectra of different NDs, (b) Deconvoluted PL spectrum for S5 sample and (c) ZPL intensity of NV^o and NV^- centers for different air oxidized samples under similar experimental conditions.

NV^o centers becomes highest at oxidation time of 6 hours. Subsequently, the intensity reduced in case of oxidation time of 8 hours. Whereas, the ZPL intensity of NV^- centers increased with the oxidation time and becomes highest for oxidation time of 6 hours (S4). For sample S5, it was nearly equal to that of sample S4. Hence, the NV^-/NV^o ratio was highest in case of sample S5. The NV^-/NV^o ratio for different samples was compared by considering the total PL intensity in the side bands of NV^o (560-630 nm) and NV^- (630-745 nm) centers. The NV^-/NV^o ratio was maximum for sample S5 (NV^-/NV^o ~ 4.5) and minimum for sample S2 (NV^-/NV^o ~ 4.2). The higher PL intensity of NV^- centers as compared to NV^o centers was due to selective removal of graphitic and other non-diamond carbon phases present at the surface of NDs. The non-diamond carbon and surface related defects were among primary reasons to reduce the stability of NV^- centers by creating electron trapping sites near the surface. With the removal of non-diamond carbon content and defects, both the concentration of stable NV^- centers as well as NV^-/NV^o ratio increased. With air oxidation, the oxygen related functionality appeared on the surface as observed from XPS analysis. The oxygen functionalization leads to higher electronegativity of the surface. The high electronegative surface provided stability to NV^- centers. Hence, as the oxidation time increased, the NV^-/NV^o ratio increased. The XPS analysis showed that the surface contained a finite amount of sp^2 carbon on the surface even after air oxidation for 8 hours. This sp^2 carbon may be completely removed through air oxidation at higher temperature. However, very high degree of oxidation is detrimental to the ensemble photo-stability of NV centers as reported in an earlier work[21].

To observe the ensemble brightness of NV centers in different samples, the confocal microscopy was

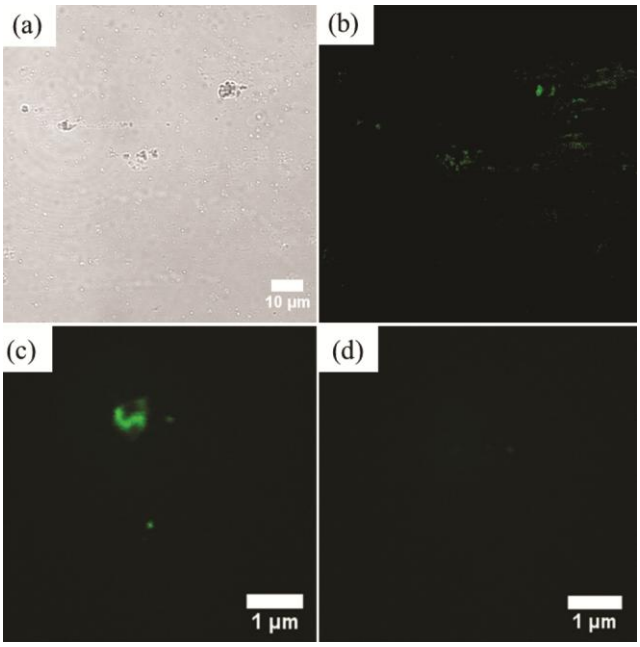

Fig. 7 — (a) and (b) shows the bright field and confocal images, respectively, for S5 sample, (c) and (d) shows the brightness of one emitting spot at laser exposure time of T = 0 sec and T ~ 5 minutes respectively. As seen in the figure, the brightness of the selected spot has been completely bleached within 5 minutes of continuous laser exposure.

carried out. As purchased sample (S1), although, exhibits some NV related emitting spots, most of the substrate was found to contain non-emitting ND agglomerates. The ensemble brightness of different samples follows the same trend as observed in PL spectra. The air oxidation leads to higher NVs related brightness of NDs. Figure 7 shows the confocal imaging of air oxidized sample; S5. The bright field image, Fig 7(a), shows the presence of ND agglomerates of non-uniform size dispersed over the cover slip. Figure 7(b) shows the confocal image of the same field of view. Most of the agglomerates contained NV related emission in the wavelength range of 550-650 nm (Fig. (b)). Hence, the air oxidation at 450 ^{o}C for 8 hours leads to bright emission due to NV enters. To analyze the ensemble photo-stability, the confocal imaging of sample S5 was carried out under continuous laser excitation. For the bleaching measurements, the laser excitation of 488 nm was used with laser power of 50mW. Figure 7(c) shows the confocal image of one of the emitting spots at laser exposure time of T = 0 sec. After ~ 5 minutes of continuous laser exposure, the brightness of the investigated spot was quenched almost completely (Fig. 7(d)). The live imaging of the investigated field of view under continuous laser excitation showed no signs of photo-blinking. The degradation of brightness was found to be gradual. This might be due to the fact that high laser power would lead to complete oxidation of the ND particles. As the size of ND particles decreased, the concentration of stable NV centers decreased and this leads to reduction in the brightness of agglomerates. Since, the bio-imaging and other ensemble related application generally requires lower laser intensity, the air oxidized sample seems to be suitable for different such applications.

4 Conclusions

The as grown NDs contain non-diamond carbon content on the surface which is not suitable to host stably emitting NV centers. Different purification techniques are explored to selectively remove these contaminations from NDs and simultaneously enhance the NV emission collection. In the present work, we have explored the effect of low temperature air oxidation (450° C) under different oxidation time on non-diamond carbon content and NV emission collection. The non-diamond carbon concentration and defects are drastically reduced upon one step air oxidation at 450° C for different oxidation times as observed from Raman spectroscopy and XPS. The crystallinity of NDs is intact during heat treatment in air with no change in the crystallite size are observed from XRD. In addition to selective removal of sp^2 carbon, the oxygen functionalities appear at the surface of NDs in case of oxidized samples as observed from XPS. The characteristic emission due to NV^o and NV^- centers is successfully observed from air oxidized NDs.

Most of the emission in different oxidized NDs found to be concentrated in the side bands of NV^- centers. Maximum emission collection and NV^-/NV^o ratio are observed for sample oxidized for 8 hours. The brightness and photo-stability of sample S5 is enhanced multifold as compared to as received NDs. Under high laser power continuous excitation, the brightness of sample S5 is bleached out within ~ 5 minutes without showing any signs of photo-blinking indicating stable emission. Under proper surface treatment, these NDs may be used for different ensemble applications which require stable and bright emission due to NV centers.

References

1 Aharonovich I, Castelletto S, Simpson D, Su C, Greentree A & Prawer S, *Rep Prog Phys,* 74 (2011) 076501.

2 Collins A T, *Diam Relat Mater,* 1 (1992) 457.

3 Hounsome L, Jones R, Martineau P, Shaw M, Briddon P, Öberg S, Blumenau A & Fujita N, *phys status solidi a*, 202 (2005) 2182.
4 Jelezko F, Tietz C, Gruber A, Popa I, Nizovtsev A, Kilin S & Wrachtrup J, *Single Molecules*, 2 (2001) 255.
5 Schirhagl R, Chang K, Loretz M & Degen C L, *Annu Rev Phys Chem*, 65 (2014) 83.
6 Hong S, Grinolds M S, Pham L M, Le Sage D, Luan L, Walsworth R L & Yacoby A, *MRS Bull*, 38 (2013) 155.
7 Gruber A, Dräbenstedt A, Tietz C, Fleury L, Wrachtrup J & Von Borczyskowski C, *Sci*, 276 (1997) 2012.
8 Chojnacki J & Eggeling C, *Retrovirology*, 15 (2018) 41.
9 Dolde F, Fedder H, Doherty M W, Nöbauer T, Rempp F, Balasubramanian G, Wolf T, Reinhard F, Hollenberg L C & Jelezko F, *Nat Phys*, 7 (2011) 459.
10 Tzeng Y-K, Tsai P-C, Liu H-Y, Chen O Y, Hsu H, Yee F-G, Chang M-S & Chang H-C, *Nano lett*, 15 (2015) 3945.
11 Hsiao W W-W, Hui Y Y, Tsai P-C & Chang H-C, *Acc Chem Res*, 49 (2016) 400.
12 Smith B R, Inglis D W, Sandnes B, Rabeau J R, Zvyagin A V, Gruber D, Noble C J, Vogel R, Ōsawa E & Plakhotnik T, *Small*, 5 (2009) 1649.
13 Mochalin V N, Shenderova O, Ho D & Gogotsi Y, *Nat Nanotechnol*, 7 (2012) 11.
14 Gaebel T, Bradac C, Chen J, Say J, Brown L, Hemmer P & Rabeau J, *Diam Relat Mater*, 21 (2012) 28.
15 Krüger A, Kataoka F, Ozawa M a a, Fujino T, Suzuki Y, Aleksenskii A, Vul A Y & Ōsawa E, *Carbon*, 43 (2005) 1722.
16 Krueger A & Lang D, *Adv Funct Mater*, 22 (2012) 890.
17 Kumar R, Pandit P, Pal P, Dhakate S, Pant R, Kumar R, Avasthi D K & Singh D K, *AIP Adv* 8 (2018) 085023.
18 Kumar R, Yoon S, Lee K, Pal P, Pant R, Suman C, Dhakate S, Kumar R, Avasthi D K & Singh D K, *RSC Adv*, 6 (2016) 47164.
19 Kumar R, Cong T T, Lee K, Pal P, Dhakate S, Kumar R, Avasthi D K & Singh D K, *Mater Res Express*, 6 (2019) 115097.
20 Fu K-M, Santori C, Barclay P & Beausoleil R, *Appl Phys Lett*, 96 (2010) 121907.
21 Kumar R, Singh D K, Kumar P, Kumar R & Dhakate S, *Diam Relat Mater*, 97 (2019) 107431.
22 Wada N & Solin S, *Physica B+ C* 105 (1981) 353.
23 Lagzdina E, Lingis D, Plukis A, Plukienė R, Gaspariūnas M, Matulaitienė I, Kovalevskij V, Niaura G & Remeikis V, *Nucl Instrum Methods Phys Res, B* 444 (2019) 23.
24 Shenderova O, Panich A, Moseenkov S, Hens S, Kuznetsov V & Vieth H-M, *J Phys Chem C* 115 (2011) 19005.
25 Fanning P E & Vannice M A, *Carbon* 31 (1993) 721.
26 Butenko Y V, Krishnamurthy S, Chakraborty A, Kuznetsov V, Dhanak V, Hunt M & Šiller L, *Phys Rev B* 71 (2005) 075420.